Inorganic Chemistry

Article

pubs.acs.org/IC

Probing the Links between Structure and Magnetism in $Sr_{2-x}Ca_xFeOsO_6$ Double Perovskites

Ryan Morrow,[†] John W. Freeland,[‡] and Patrick M. Woodward*[,†]

[†]Department of Chemistry and Biochemistry, The Ohio State University, Columbus, Ohio 43210-1185, United States

[‡]Advanced Photon Source, Argonne National Laboratory, 9700 Cass Avenue, Argonne, Illinois 60439, United States

Supporting Information

ABSTRACT: The synthesis, structure, and properties of the ordered double perovskites Sr_2FeOsO_6, Ca_2FeOsO_6, and $SrCaFeOsO_6$ are reported. The latter two compounds have monoclinic $P2_1/n$ symmetry and $a^-a^-b^+$ tilting of the octahedra, while Sr_2FeOsO_6 is tetragonal with $I4/m$ symmetry and $a^0a^0c^-$ tilting. Magnetic measurements indicate and neutron powder diffraction studies confirm that Ca_2FeOsO_6 is a ferrimagnet with a Curie temperature of 350 K. The ferrimagnetism is retained if half of the Ca^{2+} ions are replaced with larger Sr^{2+} ions to form $SrCaFeOsO_6$ (T_C = 210 K). This substitution reduces the degree of octahedral tilting, but unlike most perovskites, the magnetic ordering temperature decreases as the Fe−O−Os bond angles approach a linear geometry. In contrast, Sr_2FeOsO_6 orders antiferromagnetically, as previously reported. X-ray absorption spectroscopy confirms the assignment of Fe(III) and Os(V) oxidation states for all three compounds. In these insulating double perovskites, the magnetic ground state is governed by a competition between the four-bond Fe−O−Os−O−Fe antiferromagnetic superexchange coupling of Fe(III) ions and the two-bond Fe−O−Os antiferromagnetic superexchange coupling between neighboring Fe(III) and Os(V) ions. When the Fe−O−Os bonds are linear, as they are in the c direction in Sr_2FeOsO_6, the four-bond coupling between Fe(III) ions prevails. The competition shifts in favor of antiferromagnetic coupling of Fe(III) and Os(V) as the Fe−O−Os bond angles bend in response to chemical pressure.

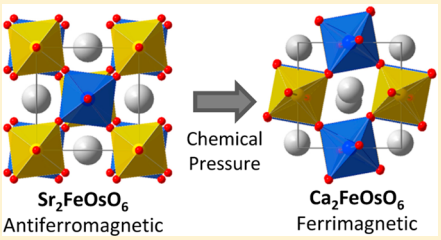

INTRODUCTION

Double perovskites, with general formula $A_2BB'O_6$, typically adopt a structure of alternating BO_6 and $B'O_6$ octahedra that mimics the pattern of cation/anion ordering seen in the rock salt structure.[1] Because of the wide variety of elemental combinations possible in this quaternary family, a considerable variety of attractive material properties can be accessed, including tunneling magnetoresistance, half metallic behavior, and high-temperature ferrimagnetism.[2−5] While the magnetic properties of metallic double perovskites such as Sr_2FeMoO_6 have been well explained by the double exchange mechanism,[6] the magnetic properties of insulating double perovskites where B is a 3d transition metal and B′ is a 4d or 5d transition metal cannot reliably be predicted[7−9] using the well-known Good-enough−Kanamori (GK) rules.[10,11]

Recently, several osmium-based double perovskites, Sr_2BOsO_6 (B═Cr, Fe, Co), which had first been prepared by Sleight et al.[12] have been studied in greater detail.[5,13,14] Each of these compounds is an insulator, and thus, their magnetic properties are dictated by superexchange interactions. While Sr_2CrOsO_6 is a ferrimagnet, in accordance with the GK rule predicting antiparallel d^3−d^3 Cr(III)−O−Os(V) superexchange coupling, Sr_2FeOsO_6 and Sr_2CoOsO_6 have been found to order antiferromagnetically despite the predicted ferromagnetic coupling of ions with d^5−d^3 and d^7−d^2 electronic configurations, respectively. In the recently reported magnetic structure of Sr_2FeOsO_6, the Fe and Os ions couple antiparallel in the ab plane, where the Fe−O−Os bond angles are bent, while a more complex coupling is observed along the c axis where the Fe−O−Os bonds are linear.[15]

The antiferromagnetic structure of Sr_2FeOsO_6 is not easily rationalized. Normally, the magnetic coupling interactions in perovskites containing d^5 and/or d^3 ions are isotropic. The presumed high spin d^5 and d^3 configurations of Fe(III) and Os(V), respectively, would seem to rule out orbital ordering. The tetragonal crystal structure of Sr_2FeOsO_6 leaves open the possibility that the individual superexchange interactions are highly sensitive to changes in the Fe−O−Os bond angles. This idea is supported by the recent report that Ca_2FeOsO_6 is a ferrimagnet rather than an antiferromagnet.[16] In this study, we use neutron diffraction to study the crystal and magnetic structure of Ca_2FeOsO_6 as a function of temperature for the first time. We have also prepared and studied $SrCaFeOsO_6$ to further explore the role of chemical pressure and octahedral tilting on the magnetic interactions in osmate double perovskites. For completeness, the crystal and magnetic structures of Sr_2FeOsO_6 are reinvestigated. The results of this comprehensive study provide important insight into how the complex magnetism of the osmate double perovskites arises from competing magnetic superexchange interactions.

Received: April 2, 2014
Published: July 15, 2014

   dx.doi.org/10.1021/ic5006715 | Inorg. Chem. 2014, 53, 7983−7992

EXPERIMENTAL SECTION

Bulk $Sr_{2-x}Ca_xFeOsO_6$ powders were synthesized by grinding stoichiometric amounts of SrO_2 (Sigma–Aldrich, 98% pure), CaO (Sigma–Aldrich, 99.9%), Fe_2O_3 (Alfa Aesar, 99.945%), and Os (Alfa Aesar, 99.98% pure) reagents with a mortar and pestle. The resultant mixture was loaded into an alumina tube that was placed into a silica tube along with an additional alumina vessel containing PbO_2, which decomposes to PbO and O_2 at elevated temperature and therefore acts as an in situ source of oxygen. A calculated excess of PbO_2 resulting in one-quarter mole excess O_2 per mole of A_2FeOsO_6 product was utilized in order to ensure the full oxidation of Os without rupturing the silica tube. The silica tube, having an approximate volume of 40 mL with 3 mm thick walls, was subsequently evacuated and sealed before being heated to 1000 °C for a period of 48 h. This reaction was performed in a box furnace located inside a fumehood. It is important to take great caution when heating Os metal or Os-containing compounds, due to the potential formation of highly toxic OsO_4 gas at high temperatures. Individual batches of the materials did not exceed 1.5 g in order to prevent explosion of the sealed silica tube due to oxygen pressure.

$$4SrO_2 + Fe_2O_3 + 2Os + (2PbO_2) \rightarrow 2Sr_2FeOsO_6 + (2PbO) + 1/2O_2$$

$$2SrO_2 + 2CaO + Fe_2O_3 + 2Os + (4PbO_2) \rightarrow 2SrCaFeOsO_6 + (4PbO) + 1/2O_2$$

$$4CaO + Fe_2O_3 + 2Os + (6PbO_2) \rightarrow 2Ca_2FeOsO_6 + (6PbO) + 1/2O_2$$

The phase purity of the resultant black powder was verified by the use of Cu Kα1 X-ray diffraction executed with a Bruker D8 Advance diffractometer equipped with a Ge(111) monochromator.

Variable temperature neutron powder diffraction experiments were conducted on the POWGEN[17] beamline at Oak Ridge National Laboratory's Spallation Neutron Source for the two end members Sr_2FeOsO_6 and Ca_2FeOsO_6. Sample sizes of approximately 1.5 g each were each contained within 8 mm vanadium cans for these experiments. Two wavelength ranges were measured at each temperature producing histograms with *d*-spacing ranges of 0.2760–3.0906 Å and 2.2076–10.3019 Å, referred to as frame 1.5 and frame 5, respectively. Long scan times of 1 h for frame 1.5 and 2 h for frame 5 were collected at 12, 100, and 300 K while brief 5 min scans were collected in each frame at 10 K intervals for Sr_2FeOsO_6. Equivalent times and frames were used for Ca_2FeOsO_6 at temperatures of 10, 100, 200, 300, and 400 K as well as at 10 K for $SrCaFeOsO_6$. Rietveld refinements were conducted with the aid of GSAS EXPGUI,[18,19] and the magnetic form factors for Os, which were not included within the software database, were manually entered by the use of coefficients listed by Kobayashi et al.[20]

The magnetic susceptibilities of Sr_2FeOsO_6, $SrCaFeOsO_6$, and Ca_2FeOsO_6 were collected within the temperature range 5–400 K with both zero-field-cooled and field-cooled conditions under an applied field of 1 kG. Additional field dependence measurements between fields of +5 and −5 T were conducted for $SrCaFeOsO_6$ at 5 K and for Ca_2FeOsO_6 at 5 and 300 K. These measurements were accomplished utilizing a Quantum Design MPMS SQUID magnetometer. All samples were contained in gelatin capsules and mounted in straws for insertion into the instrument. No diamagnetic corrections for the sample holder were taken into account.

Sr_2FeOsO_6 and Ca_2FeOsO_6 powders were pressed into pellets prior to being sintered at 1100 °C, after which they were cut into a bar shape for electrical transport measurements. The density was calculated to be 63% and 54% of the theoretical densities of the materials, respectively. Four equally spaced indium wire point contacts were secured to the pellet with silver paint before DC resistivity measurements were carried out utilizing a Quantum Design model 6000 PPMS over the temperature ranges 160–350 K for Sr_2FeOsO_6 and 100–400 K for Ca_2FeOsO_6. At lower temperatures, the samples became too resistive to accurately measure the intrinsic resistivity.

X-ray absorption spectroscopy (XAS) measurements were conducted for Sr_2FeOsO_6, $SrCaFeOsO_6$, and Ca_2FeOsO_6 at the 4-ID-C beamline of the Advanced Photon Source. XAS measurements were conducted at the Fe $L_{3,2}$ edges at a temperature of 20 K for Sr_2FeOsO_6 and at 10 K for $SrCaFeOsO_6$ and Ca_2FeOsO_6. The energy scales of all the XAS were aligned with the use of an Fe standard acquired simultaneously.

RESULTS

Crystal Structure. In double perovskites, antisite mixing of the cations that reside on the octahedral sites is always a possibility, particularly when the difference in oxidation states is 2 or less.[21] To investigate this possibility, the Fe/Os cation order parameter was determined from Rietveld refinements of X-ray diffraction data, where the contrast between the scattering power of Fe and Os is much larger than it is for neutron diffraction.[22] The order parameter is defined as $\eta = 2\theta - 1$, where θ is the occupancy of Fe on the site that is predominantly occupied by Fe (or the occupancy of Os on the site predominantly occupied by Os). Our refinements gave order parameters of 76.2(4)%, 97.0(3)%, and 80.6(5)% for Sr_2FeOsO_6, $SrCaFeOsO_6$, and Ca_2FeOsO_6, respectively. Order parameters of 88.0(2)% and 90% were previously reported for Sr_2FeOsO_6 and Ca_2FeOsO_6, respectively.[13,16] Our samples show slightly lower levels of Fe/Os ordering, although interestingly, the $SrCaFeOsO_6$ compound is almost completely ordered. In perovskites with partial ordering, it is not unusual for the degree of antisite mixing to be sensitive to variations in synthesis conditions.[21] The X-ray refinements did not indicate any appreciable deviation in the overall stoichiometry due to loss of Os.

Refinements using neutron powder diffraction data show that Sr_2FeOsO_6 crystallizes with tetragonal *I*4/*m* space group symmetry at room temperature, in agreement with recent reports (see Figure 1).[13,23] This distortion from the high-symmetry cubic aristotype structure is usually driven by out-of-phase octahedral tilting about the *c* axis ($a^0a^0c^-$ tilting), although it also permits a tetragonal distortion of the octahedra. It is adopted by a number of double perovskites, including Sr_2CoOsO_6, Sr_2NiOsO_6, and Sr_2CoReO_6.[14,24,25] No structural phase transitions were observed over the temperature range investigated. Further details concerning the quality of refinement fit and structure can be found in Supporting Table 1 (Supporting Information).

The evolution of the lattice parameters of Sr_2FeOsO_6, plotted in Figure 1c, show an increasing degree of tetragonal distortion as the temperature decreases. The lattice parameters evolve linearly on cooling from room temperature to the Néel temperature of 140 K,[13] below which there is a nonlinear increase in *c* and a corresponding decrease in *a*. The correspondence between magnetic ordering and a change in the degree of tetragonal distortion indicate significant magnetostriction. The evolution of octahedral tilting, the unit cell volume, and the diffraction patterns are presented in the Supporting Information. There is no discontinuity in the octahedral tilt angle as a function of temperature. Furthermore, the Os(V) centered octahedra remain symmetric, that is to say the Os–O1 and Os–O2 distances are equivalent to each other within experimental uncertainty (and the O–Os–O angles are all 90° by symmetry), which suggests that the magnetostriction is primarily associated with an increased tetragonal distortion of the Fe(III) centered octahedra. The observation that octahedra

dx.doi.org/10.1021/ic5006715 | Inorg. Chem. 2014, 53, 7983–7992

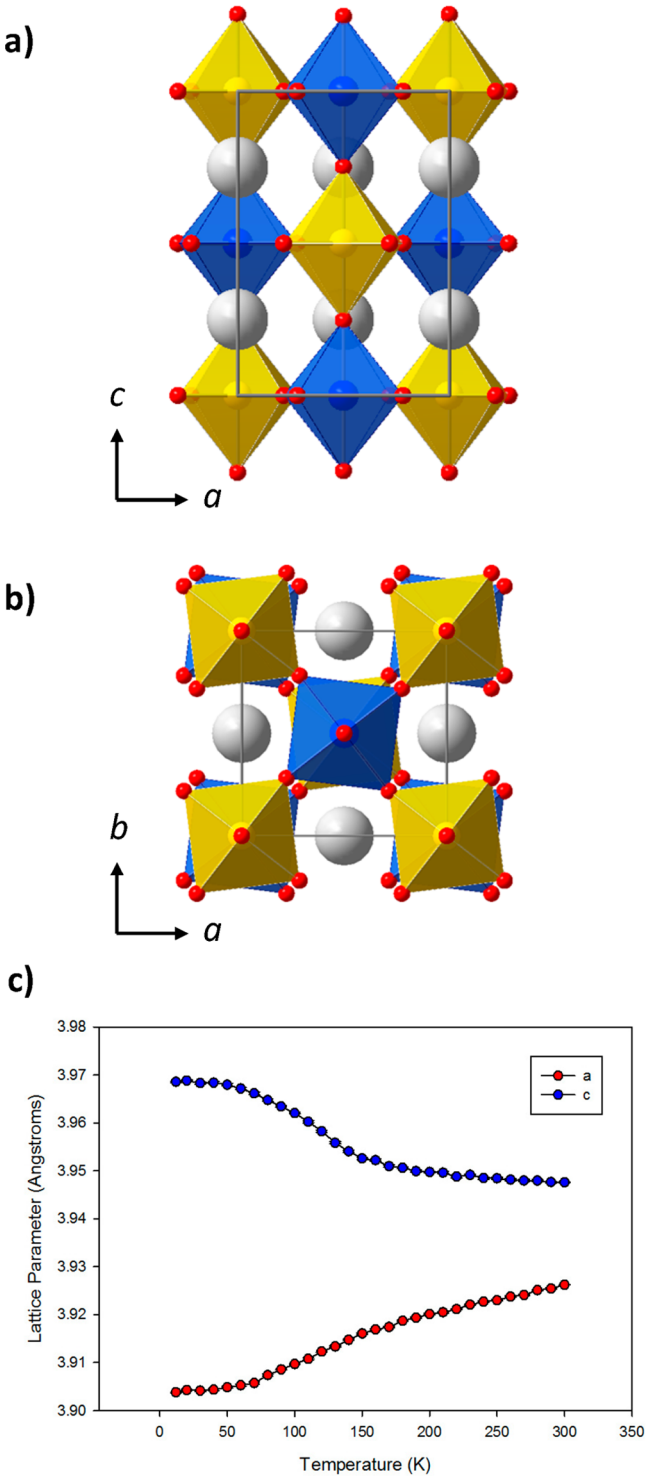

Figure 1. Tetragonal crystal structure of Sr_2FeOsO_6 at 12 K as viewed (a) looking down the *b* axis and (b) looking down the *c* axis. The blue octahedra contain predominantly osmium, while the yellow ocathedra contain primarily iron. The strontium and oxygen atoms are shown as gray and red spheres, respectively. (c) The *a* and *c* lattice parameters of Sr_2FeOsO_6 as a function of temperature. Error bars are smaller than the symbols.

containing a high spin d^5 Fe(III) ion become distorted at low temperature is somewhat surprising, but it is in agreement with the earlier synchrotron and neutron measurements of Paul et al.[13,15]

Attempts were made to refine the structure of Sr_2FeOsO_6 at low temperatures in the space group *I*4 using the structural model given in the Supporting Information of Paul et al.[15] In this model, pairs of Fe and Os ions are allowed to move toward each other along the *c* axis in order to produce dimerization. Paul et al. report shifts in fractional coordinates of 0.0030(16) (neutron data) and 0.0044(3) (synchrotron data) away from the higher symmetry positions mandated by the *I*4/*m* symmetry, leading to a slight improvement of fit quality. Our refinements result in a comparable displacement, 0.0033(27), but the reduction of R_P is only from 3.21% to 3.20%. Given the marginal improvement in the goodness of fit and the fact that the shift is of the same order of magnitude as the estimated standard deviation, we do not find conclusive evidence to support the dimerization model and *I*4 symmetry.

$SrCaFeOsO_6$ and Ca_2FeOsO_6 were both found to be monoclinic, having a space group of $P2_1/n$, the most common space group for monoclinic double perovskites.[26] Ca_2FeOsO_6 did not undergo observable phase transitions over the temperature range 10−400 K for which neutron powder diffraction measurements were conducted. The structure of this compound is shown in Figure 2. Refined bond lengths and

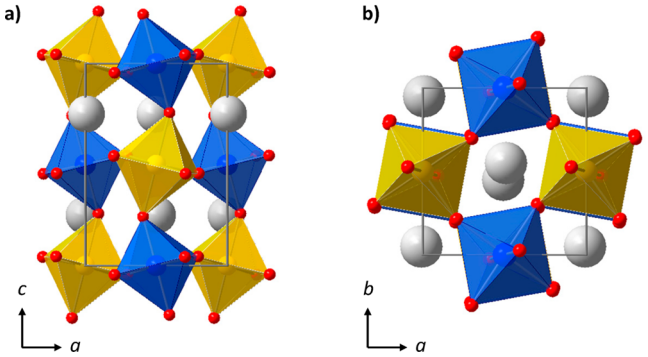

Figure 2. Monoclinic crystal structure of Ca_2FeOsO_6 at 10 K as viewed (a) looking down the *b* axis and (b) looking down the *c* axis. The blue octahedra contain predominantly osmium, while the yellow ocathedra contain predominantly iron. The strontium and oxygen atoms are shown as gray and red spheres, respectively.

angles at select temperatures can be found in Table 1, and refined frame 1.5 neutron powder diffraction patterns of Ca_2FeOsO_6 at 10 and 400 K can be found in Figure 3. Here, we see an even more pronounced tetragonal distortion of the iron octahedra, involving an expansion of the two Fe−O3 bonds that lie along one axis of the octahedron, and a compression of the other four Fe−O bonds. Unlike Sr_2FeOsO_6, the Os(V) octahedra also distort on cooling, with a distortion that is the inverse of the Fe(III) octahedra: two Os(V)−O bonds contract and the other four expand. $SrCaFeOsO_6$ also contains octahedra that have similar distortions at 10 K, although to a lesser degree. The average ∠Fe−O−Os bond angle in $SrCaFeOsO_6$ is 158.9° while the angle in Ca_2FeOsO_6 is 150.9°; thus, the bond angles in $SrCaFeOsO_6$ represent a scenario of intermediate octahedral tilting between the end members of the series.

X-ray Absorption Spectroscopy. The oxidation states of the transition metals were determined through a combination of XAS and bond length analysis. Bond valence sums for Fe (see Table 1 and Supporting Information, Table 1) are all in the range 3.2−3.3, suggesting a 3+ oxidation state, and the

dx.doi.org/10.1021/ic5006715 | Inorg. Chem. 2014, 53, 7983−7992

Table 1. Refinement Parameters for $SrCaFeOsO_6$ and Ca_2FeOsO_6 from Neutron Powder Diffraction Data

	$SrCaFeOsO_6$	Ca_2FeOsO_6				
	10 K	10 K	100 K	200 K	300 K	400 K
space group	$P2_1/n$	$P2_1/n$	$P2_1/n$	$P2_1/n$	$P2_1/n$	$P2_1/n$
a (Å)	5.4998(1)	5.3870(2)	5.3885(2)	5.3920(2)	5.4004(1)	5.4079(2)
b (Å)	5.5112(1)	5.4951(2)	5.4954(1)	5.4944(2)	5.4957(1)	5.4977(2)
c (Å)	7.7784(2)	7.6657(3)	7.6689(2)	7.6731(3)	7.6820(2)	7.6899(3)
V (Å)^3	235.769(6)	226.92(1)	227.09(1)	227.32 (18)	227.995(9)	228.63(2)
β	89.917(3)	90.010(7)	90.021(9)	90.01(1)	90.028(7)	90.012(5)
R_{wp}	3.25	2.58	1.21	2.14	1.14	1.76
R_p	9.20	2.18	1.10	2.04	1.02	1.56
Ca x	−0.0046(6)	0.0084(10)	0.0085(7)	0.0101(7)	0.0075(8)	0.0039(9)
Ca y	0.0266(2)	−0.0500(4)	−0.0488(3)	−0.0477(3)	−0.0464(3)	−0.0459(3)
Ca z	0.2499(6)	0.249(16)	0.2531(16)	0.249(2)	0.254(13)	0.252(14)
O1 x	0.2244(5)	0.2059(10)	0.2045(11)	0.200(13)	0.2015(12)	0.2090(8)
O1 y	0.2221(7)	0.2134(8)	0.2102(9)	0.201(1)	0.2013(10)	0.2114(8)
O1 z	−0.0277(3)	0.0453(7)	0.0447(9)	0.0425(9)	0.0416(9)	0.0426(7)
O2 x	0.2085(5)	0.201(11)	0.2002(11)	0.206(13)	0.205(12)	0.1998(8)
O2 y	0.2116(6)	0.1977(8)	0.1998(9)	0.209(1)	0.2092(9)	0.2000(8)
O2 z	0.5376(4)	0.4567(7)	0.4563(9)	0.4538(9)	0.4557(9)	0.4604(7)
O3 x	0.4352(4)	0.5927(6)	0.5894(4)	0.5867(4)	0.5848(4)	0.5864(5)
O3 y	−0.0119(3)	0.0262(5)	0.0249(4)	0.0247(4)	0.0238(4)	0.0236(4)
O3 z	0.2515(6)	0.2426(8)	0.2446(9)	0.247(12)	0.247(11)	0.2447(8)
Ca U_{iso}	0.0052(1)	0.0083(4)	0.0088(4)	0.0107(3)	0.0119(4)	0.0148(4)
Fe = Os U_{iso}	0.00233(4)	0.0042(2)	0.0045(1)	0.0057(1)	0.00602(8)	0.0085(2)
O U_{iso}[a]	0.00618(8)	0.0064(2)	0.071(17)	0.087(17)	0.094(14)	0.0114(3)
Fe−O1 (×2)	1.978(4)	1.957(5)	1.967(5)	1.991(6)	1.995(6)	1.975(4)
Fe−O2 (×2)	2.003(3)	1.969(5)	1.982(5)	1.989(7)	1.994(6)	1.984(4)
Fe−O3 (×2)	1.967(5)	2.040 (6)	2.022(7)	1.998(10)	2.000(8)	2.023(6)
Os−O1 (×2)	1.960(4)	2.002(5)	1.997(5)	1.986(7)	1.981(7)	1.984(4)
Os−O2 (×2)	1.982(4)	2.012(5)	1.999(5)	1.979(6)	1.973(6)	1.995(5)
Os−O3 (×2)	1.990(5)	1.931(6)	1.941(6)	1.960(9)	1.957(8)	1.943(6)
∠Fe−O1−Os	162.5(1)	152.8(3)	152.3(3)	150.9(4)	151.3(2)	153.8(3)
∠Fe−O2−Os	155.3(1)	150.3(3)	150.3(3)	151.9(4)	152.3(3)	151.4(2)
∠Fe−O3−Os	158.9(1)	149.6(2)	150.7(1)	151.5(1)	152.1(1)	151.7(1)
Fe BVS	3.28	3.24	3.22	3.19	3.16	3.18

[a]The U_{iso} values for all three oxygen atoms were constrained to be equal.

average Fe−O bond length agrees well with the values expected from ionic radii for Fe(III).[27,28] Yet, the observed distortions of the octahedra are unusual for the d^5 Fe(III) and d^3 Os(V) ions, so XAS measurements were used to verify the oxidation state assignments. Figure 4 shows the XAS near edge peak shape and energy along with standards for Fe(III), Fe(II), and Fe. The standards used were $LaFeO_3$, $FeTiO_3$, and metallic Fe film. A comparison leaves little doubt that Fe(III) is the correct assignment. The Os bond valence sums are less reliable due to the simple fact that fewer examples of Os compounds exist; nonetheless, direct comparison of the average Os−O bond length with Sr_2CrOsO_6[5] and Sr_2NiOsO_6,[24] which contain Os(V) and Os(VI), respectively, support the assignment Os(V) in Sr_2FeOsO_6, $SrCaFeOsO_6$, and Ca_2FeOsO_6.

Electrical and Magnetic Properties. The DC resistivities of Sr_2FeOsO_6 and Ca_2FeOsO_6 were measured, and an exponential increase in resistivity with decreasing temperature was observed for both materials, indicating the insulating nature of the material. A linear fit is obtained when log conductivity was plotted versus temperature raised to the $-^1/_4$ power, as shown in Figure 5. This fit is indicative of a Mott variable range hopping transport mechanism,[29] signaling localized electrons. The absolute value of the conductivity is roughly 4 orders of magnitude higher for Ca_2FeOsO_6 than it is for Sr_2FeOsO_6.

The measured magnetic susceptibility of Sr_2FeOsO_6 is shown in Figure 6. An antiferromagnetic transition is clearly visible with a Néel temperature of approximately 65 K. Paul et al.[13] reported a second antiferromagnetic transition near 140 K in a similar measuring field. That feature is not readily evident here, but we do see a deviation in the inverse susceptibility from Curie−Weiss behavior at a similar temperature. This feature becomes more apparent when considering the Fisher heat capacity,[30] shown in Figure 7, where the magnetic heat capacity begins to rise on cooling near 140 K to produce a broad feature peaking at 80 K before a sharp peak centered at 62 K. In the paramagnetic region, linear Curie−Weiss behavior is observed. From this linear fit spanning the data range from 300 to 400 K, the Curie constant was determined and used to calculate an effective moment of 4.84 μ_B per formula unit. Given the oxidation states of 3+ and 5+ for Fe and Os, respectively, and assuming a high spin state for Fe(III), the spin only effective moment should be 7.07 μ_B per formula unit. The observed effective moment is clearly much less than that of the spin only calculation. It is unlikely that spin−orbit coupling could cause such a remarkable decrease in effective moment with this electronic configuration, because the spin−orbit coupling should be quenched for the high spin d^5 Fe^{3+} ion and the effective moment for this ion alone is 5.92 μ_B. Nonetheless, our

dx.doi.org/10.1021/ic5006715 | Inorg. Chem. 2014, 53, 7983−7992

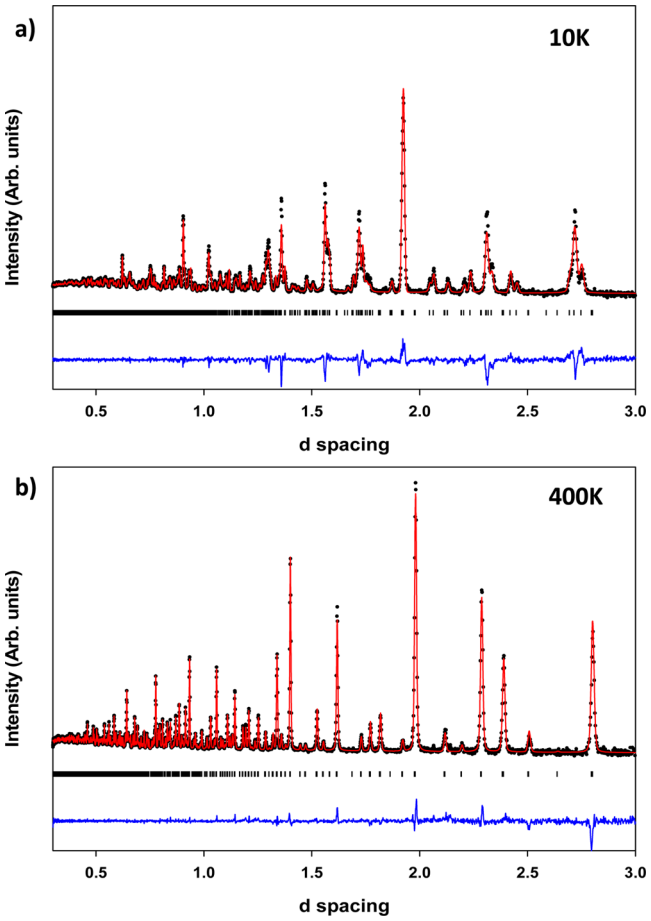

Figure 3. Refined frame 1.5 neutron powder diffraction pattern of Ca_2FeOsO_6 at (a) 10 K and (b) 400 K.

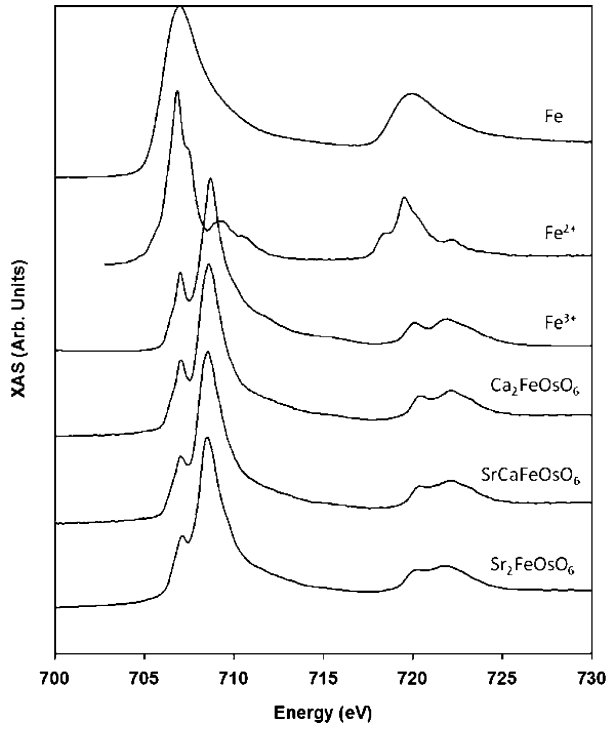

Figure 4. X-ray absorption spectrum at Fe $L_{3,2}$ edges collected for each $Sr_{2-x}Ca_xFeOsO_6$ sample as compared to standard spectra for potential oxidation states of 3+ ($LaFeO_3$), 2+ ($FeTiO_3$), and 0 (Fe). The data clearly align with the Fe^{3+} standard energy and shape.

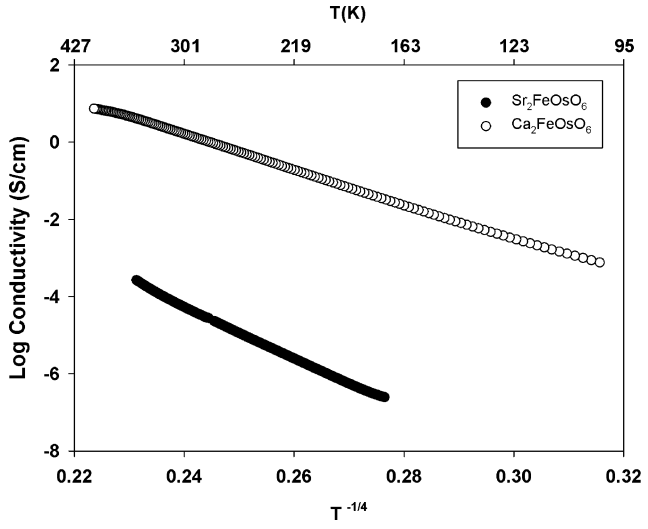

Figure 5. Temperature dependence of the electrical conductivity of Sr_2FeOsO_6 and Ca_2FeOsO_6. The linear relationship between log σ and $T^{-1/4}$ indicates a variable range hopping mechanism.

unexpectedly low value of the effective moment is similar to the values of 4.32 and 4.48 μ_B reported in the literature.[13,24] This may indicate non-negligible short-range coupling between ions at temperatures higher than the Néel temperature. From the Curie–Weiss fit, a Weiss temperature of +24 K was calculated. This is also unusual because a positive Weiss temperature is generally associated with dominant ferromagnetic interactions.

The magnetic susceptibilities of $SrCaFeOsO_6$ and Ca_2FeOsO_6, are shown in Figure 8. They indicate ferromagnetic transitions with Curie temperatures of approximately 210 and 350 K, respectively. There was not sufficient data above the transition temperatures of these compounds to produce reliable Curie–Weiss fits. There is a significant divergence between the field-cooled and zero-field-cooled susceptibility data, indicating behavior more complex than expected for a simple ferrimagnet. We hypothesize that this behavior is due to the presence of competing magnetic exchange interactions. It is also possible that Fe/Os disorder leads to the formation of clusters that give rise to the divergence between field-cooled and zero-field-cooled susceptibilities.

Figure 9 shows the hysteresis in the net magnetization confirming a ferri-/ferromagnetic component. At low temperature, the saturation magnetization values of $SrCaFeOsO_6$ and Ca_2FeOsO_6 are 1.74 and 0.97 μ_B per formula unit, respectively. These values are clearly inconsistent with the assignment of ferromagnetism, which would yield an expected M_{sat} of approximately 8 μ_B per formula unit, assuming the spin only values of 5 μ_B for Fe(III) and 3 μ_B for Os(V). On the other hand, ferrimagnetism would lead to an anticipated M_{sat} of 2 μ_B per formula unit that is in reasonably good agreement with the value obtained for $SrCaFeOsO_6$. The lower M_{sat} of Ca_2FeOsO_6 can be partially explained by considering that the Fe/Os ordering was refined to be 80.6(5)% as compared to 97.0(3)% in $SrCaFeOsO_6$. Assuming the orientation of the spin on an antisite keeps the orientation of the other ions on that crystallographic site (i.e., an Fe(III) ion sitting on an Os(V) site would have a spin that is parallel to the other osmium spins, which is antiparallel to the spins of the iron sublattice), the

dx.doi.org/10.1021/ic5006715 | Inorg. Chem. 2014, 53, 7983–7992

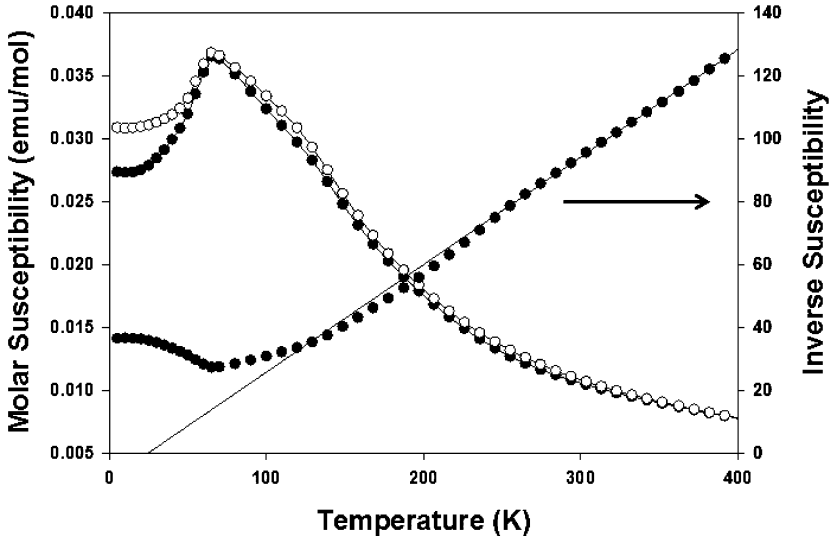

Figure 6. Molar susceptibility versus temperature data in both zero-field-cooled (filled circles) and field-cooled (unfilled circles, 1 kOe) conditions measured under an applied field of 1 kOe. The inverse of the susceptibility is plotted against the right axis, showing the linear Curie–Weiss fit.

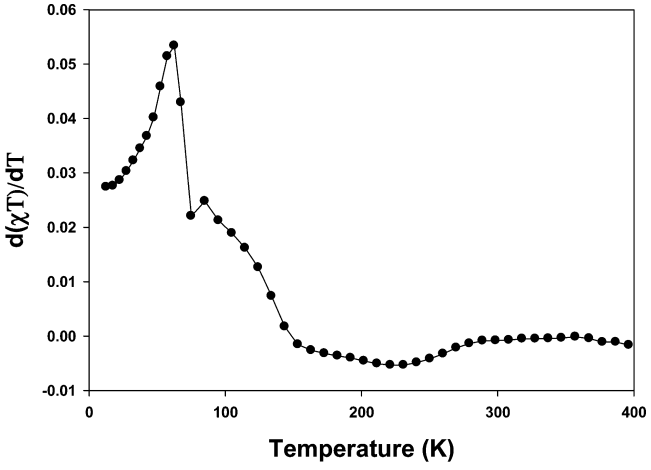

Figure 7. Temperature dependence of Fisher heat capacity of Sr_2FeOsO_6.

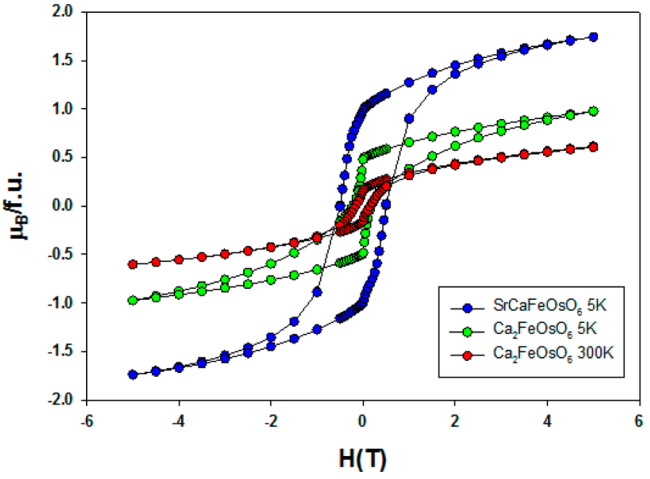

Figure 9. Field-dependent magnetization loops for $SrCaFeOsO_6$ at 5 K and Ca_2FeOsO_6 at 5 and 300 K. Magnetization units are Bohr magneton per formula unit.

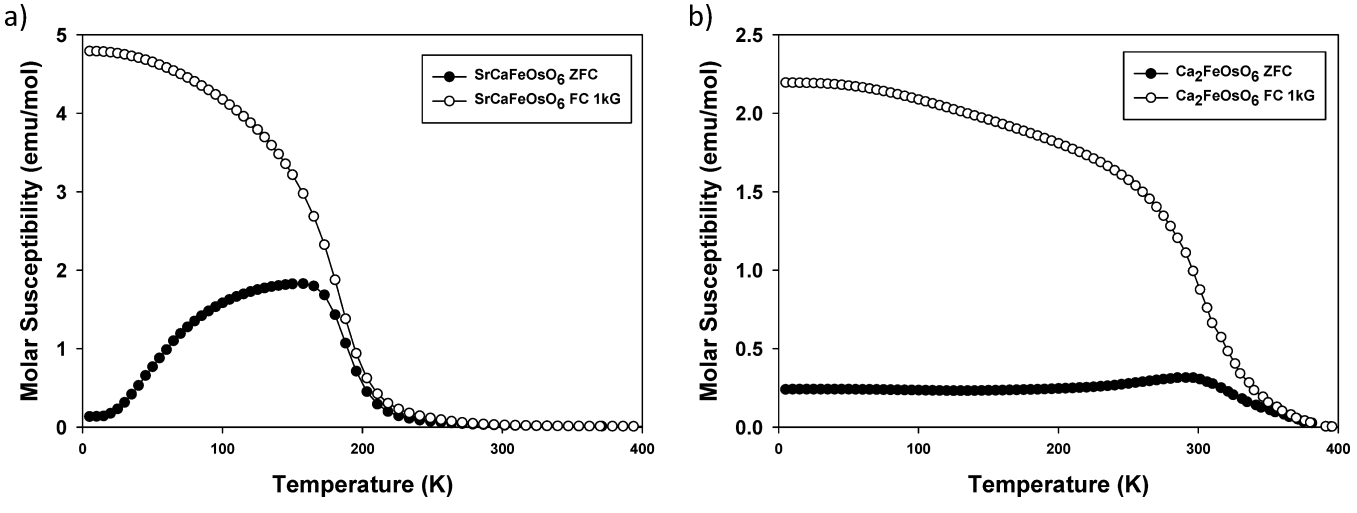

Figure 8. Molar susceptibility versus temperature of (a) $SrCaFeOsO_6$ and (b) Ca_2FeOsO_6 under field-cooled (1 kOe) and zero-field-cooled conditions, measured under an applied field of 1 kOe.

dx.doi.org/10.1021/ic5006715 | Inorg. Chem. 2014, 53, 7983–7992

antisite disorder would be expected to reduce the moment from 2.0 to 1.6 μ_B per formula unit. Thus, the smaller than expected value of M_{sat} seen for Ca_2FeOsO_6 cannot be entirely attributed to antisite disorder. It should also be noted that none of the hysteresis loops completely saturates. The hysteresis of Ca_2FeOsO_6 at 300 K clearly indicates net magnetization at room temperature, although with a reduced magnetization with respect to the value at 5 K, as expected based on the susceptibility curve (Figure 8).

A paper reporting the synthesis and magnetism of Ca_2FeOsO_6 came out just prior to the submission of this paper.[16] In that communication, Feng et al. report a Curie temperature of 320 K, which is lower than our value of 350 K, and a saturation magnetization of 1.2 μ_B/f.u. which is about 20% larger than our value of 0.97 μ_B/f.u. The discrepancies in both the T_C and the M_S values are likely to be at least partially related to differences in the Fe/Os order parameter.

Magnetic Structure. The neutron powder diffraction pattern collected on the Sr_2FeOsO_6 sample at 100 K revealed the presence of additional reflections that were able to be indexed on the nuclear cell. These peaks confirm the long-range magnetic order hinted at in the magnetic susceptibility. The magnetic Bragg peaks are the same as those reported by Paul et al.[15] and could be fit using the same magnetic structure model, resulting in refined moments of 2.0(2) and 0.4(1) μ_B for Fe and Os, respectively. These values are in close agreement with the previously reported values.

Below the lower Neél temperature of 65 K, several new diffraction peaks appear at high d spacings in the diffraction pattern of Sr_2FeOsO_6, as shown in Figure 10. At the same time,

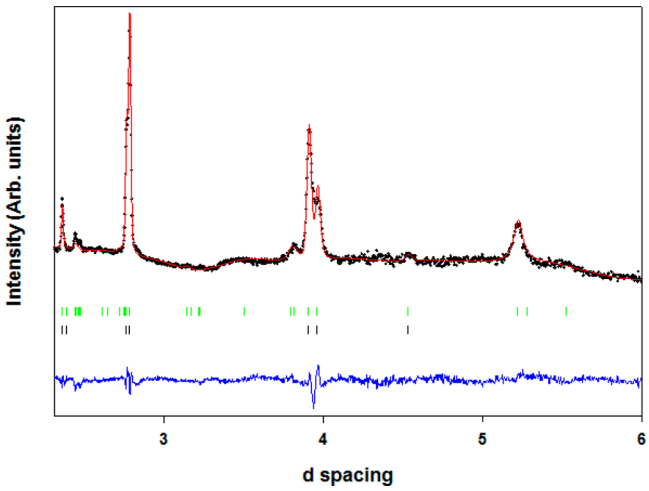

Figure 10. Refined 12 K frame 5 neutron powder diffraction histogram of Sr_2FeOsO_6 with black hash lines indicating the nuclear phase and green hashes indicating allowed magnetic phase reflections.

the magnetic reflections observed at 100 K can no longer be observed. A commensurate k vector of (0, 0, $^1/_2$) can be readily determined from these peaks, resulting in the magnetic structure shown in Figure 12a. Refinement of the Fe moment resulted in a moment of 1.86(3) μ_B per atom. Allowing the Os moment to refine leads to a negligibly small value, 0.27(3) μ_B, which points in the opposite direction of Fe moments within the same *ab* plane. These values are considerably smaller than the values of 3.07 and 0.68 μ_B reported by Paul et al.,[15] despite the higher temperature magnetic structure values being in agreement with their study. The reason behind the discrepancy in refined moments is not clear; however, it is possible that differences in antisite disorder could be partially responsible.

In the diffraction patterns of Ca_2FeOsO_6 below its Curie temperature a magnetic contribution to some of the diffraction peaks can be seen, as shown in Figure 11. Representational

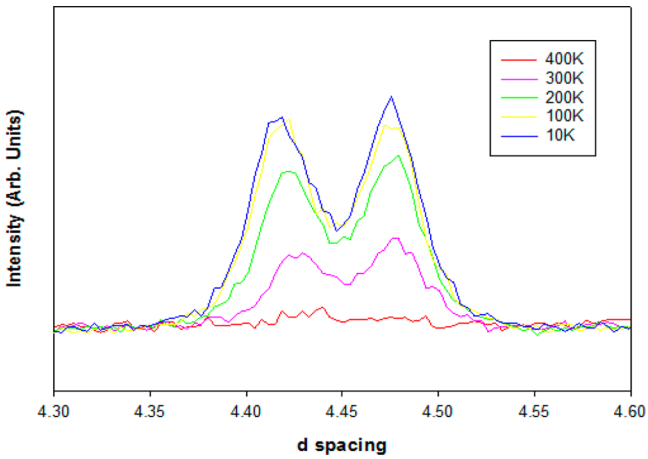

Figure 11. Increasing neutron powder diffraction intensity with the reduction of temperature of the (101) and (011) reflections revealing the onset of ferrimagnetic ordering in Ca_2FeOsO_6.

analysis was used to determine potential moment orientations, followed by trial and error to find an appropriate model, resulting in moments oriented parallel to the *c* axis. While the magnetic contribution to the intensities of these and other Bragg peaks could be successfully fit using a ferrimagnetic model, there was a very high degree of correlation between the magnitude of the Fe and Os moments. In order to extract some information about the magnitude of the ordered magnetic moments, the moment on Os was fixed, and the Fe moment was refined. The moments were always of opposite sign, and the difference between these two moments was consistently in the range 4−4.5 μ_B. Three possible solutions are as follows: (1) refinement of a moment only on Fe led to a value of 4.47(5) μ_B; (2) refinements where the Os moment was fixed at −0.5 μ_B led to an Fe moment of 3.95(5) μ_B; and (3) refinements where the Os moment was fixed at −1.5 μ_B resulted in an Fe moment of 2.58(5) μ_B.

The model 1 refinement results do have some attractive features. The negligibly small Os moment is consistent with our refinements of a very small Os moment in Sr_2FeOsO_6, and the Fe moment of 4.47 μ_B is not unusual for Fe^{3+}. However, we reject this model because it leads to saturation magnetizations in excess of 4 μ_B per formula unit, much higher than the observed value. The refinement of the Fe moment with an Os moment of −1.5 μ_B (model 3) is taken as the most realistic model as it corresponds to an M_{sat} that is similar to the measured value of 0.97 μ_B per formula unit. The reduced magnetic moments can be rationalized by considering the effects of potential spin−orbit coupling and covalency in Os^{5+} as well as the implications of disorder on the lattice reducing the magnetic scattering. It is worth noting that we observed an additional reflection, found at a d spacing of approximately 6.98 Å, in the 10 and 100 K diffraction patterns of Ca_2FeOsO_6. We were unable to match this additional peak to any known magnetic impurity or to index it by increasing the size of the magnetic cell.

dx.doi.org/10.1021/ic5006715 | Inorg. Chem. 2014, 53, 7983−7992

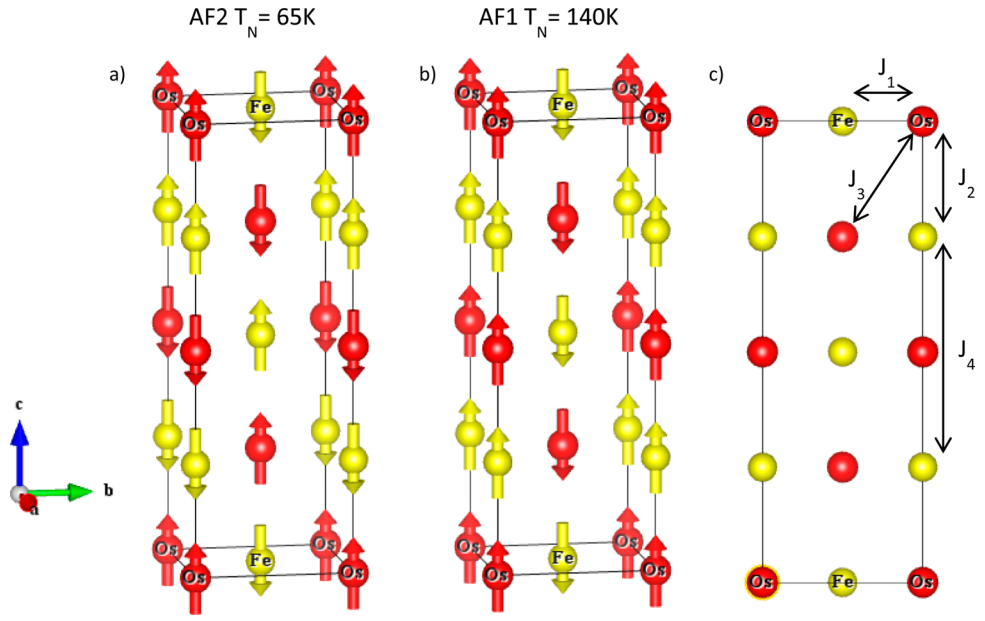

Figure 12. Magnetic structure of Sr_2FeOsO_6 (a) as determined at 12 K and (b) at 140 K. (c) The competing superexchange interactions that are discussed in the text. Sr and O ions have been omitted for clarity.

The magnetic structure of $SrCaFeOsO_6$, which contained substantial magnetic scattering contributions to the same Bragg peaks as Ca_2FeOsO_6, could be refined using the same model. As before, correlations necessitated the use of a fixed Os moment; however, the difference in the moments was larger in the case of $SrCaFeOsO_6$, approximately 6.5 μ_B. This resulted in one model with magnetic moments of 4.5(1) μ_B for Fe and a fixed moment of 2.0 μ_B for Os, values that are quite reasonable for ions that have five and three unpaired electrons, respectively. An identical fit can be obtained by fixing the Os moment at 2.25 μ_B and allowing the Fe moment to refine to a value of 4.3(1) μ_B. These values correspond to an M_{sat} close to 2 μ_B/f.u., which is in line with the value obtained by magnetometry. One would expect similar moments for Ca_2FeOsO_6 and $SrCaFeOsO_6$, given the fact that both are ferrimagnets with monoclinic symmetry. The difference in the moments obtained from analyzing the neutron diffraction patterns highlights the impact of antisite disorder on the refined magnetic moments. This result suggests the presence of higher levels of antisite disorder may play a large role in explaining the unusual magnetic moments obtained for Ca_2FeOsO_6 and Sr_2FeOsO_6.

DISCUSSION

The low-temperature magnetic structure of Sr_2FeOsO_6, as shown in Figure 12a, can be explained by considering the superexchange pathways of potential importance and the relevant Fe−O−Os bond angles for those pathways. Within the *ab* plane, octahedral tilting results in bond angles that are approximately 165°, and nearest neighbor Fe−O−Os superexchange, shown as J_1 in Figure 11c, leads to antiparallel coupling of Fe and Os spins. The situation along the *c* axis is quite different, with each Fe spin coupling parallel with one neighboring Os and antiparallel to the other. Paul et al. explain this coupling by proposing a structural distortion that leads to two different Fe−O−Os bond distances along the linear chains that run parallel to the *c* axis.[15] The Os spins couple antiparallel to the Fe that is its closest neighbor and parallel to the Fe that is slightly further away. We were not able to find evidence to support this type of dimerization in our data, yet we obtain essentially the same low-temperature magnetic structure. An alternate explanation for this structure is one where the four-bond Fe−O−Os−O−Fe exchange interaction along the *c* axis (J_4) dominates and leads to antiparallel coupling of Fe spins along these chains. This explanation is particularly compelling considering the recent report of the magnetic structure of Sr_2CoOsO_6 where four-bond Co−O−Os−O−Co superexchange is found to be unexpectedly strong.[14] In double perovskites where the 4d or 5d transition metal is a nonmagnetic d^0 cation, such as Sr_2CoWO_6[31] or Sr_2CoMoO_6,[32] antiferromagnetic coupling between the 3d transition metals via such a four-bond exchange mechanism is regularly observed.

The higher-temperature AFM structure (T_N = 140 K) shown in Figure 12b where all of the Fe and Os ions along one of these chains couple parallel to each other cannot be explained in this way. We propose that the ferrimagnetic *ab* planes are coupled to neighboring planes not by a ferromagnetic Fe−O−Os exchange (J_2) along the *c* axis but by 90° AFM Os−O−O−Os interaction (J_3) on the face-centered cubic (fcc)-type Os sublattice. This exchange pathway, which should not be neglected when 5d orbitals are concerned, would favor antiparallel coupling of Os spins. In the magnetic structure shown in Figure 12b, each osmium ion couples antiparallel to eight nearest neighbor Os ions and parallel to four nearest neighbor Os ions. Given the frustration of the fcc Os sublattice, this is the optimal configuration if the 90° Os−O−O−Os antiferromagnetic coupling across a face diagonal of the cubic unit cell is sufficiently strong. Upon cooling to the lower-temperature magnetic structure, J_4 superexchange leads to a rearrangement of the spins to form the low-temperature magnetic structure shown in Figure 12a. In this structure, each Os ion is aligned parallel with eight and antiparallel with four nearest neighbor Os spins. This is unfavorable in terms of the AFM J_3 exchange interactions.

Upon replacing strontium with the smaller calcium, the symmetry is lowered, and the Fe−O−Os bonds become bent in

dx.doi.org/10.1021/ic5006715 | Inorg. Chem. 2014, 53, 7983−7992

all directions. We hypothesize that this distortion reduces the strength of the J_4 superexchange interaction sufficiently that antiparallel Fe−O−Os coupling, J_1 and J_2, prevails in all three directions, leading to a ferrimagnetic ground state. The notion that long-range magnetic coupling pathways (i.e., 180 ° Fe−O−Os−O−Fe and 90° Os−O−O−Os interactions) effectively compete with the nearest neighbor Fe−O−Os coupling helps to explain the rather curious observation that Ca_2FeOsO_6 has a higher Curie temperature (T_C = 350 K) than $SrCaFeOsO_6$ (T_C = 210 K), despite the fact that the Fe−O−Os bonds are more highly bent in Ca_2FeOsO_6. Normally in perovskites, the strength of the nearest neighbor superexchange coupling and the temperature at which cooperative magnetic ordering occurs both decrease as the bonds becoming increasingly bent. As an example of this consider the decrease of T_N from 290 to 141 K upon going from $LaCrO_3$ to $YCrO_3$ where the Cr−O−Cr bond angles are more highly bent due to the smaller radius of the Y^{3+} cation (with respect to the La^{3+} cation).[33,34] In the $Sr_{2-x}Ca_xFeOsO_6$ system, the picture is more complicated due to the competing superexchange pathways. The Fe−O−Os bond angles in Ca_2FeOsO_6 are more bent than in $SrCaFeOsO_6$, which suppresses the longer-range superexchange interactions, allowing the nearest neighbor Fe−O−Os coupling to dominate, thereby raising T_C.

CONCLUSION

The structure and properties of double perovskites Ca_2FeOsO_6, $SrCaFeOsO_6$, and Sr_2FeOsO_6 have been reported. Sr_2FeOsO_6 is a tetragonal antiferromagnet (T_{N1} = 140; T_{N2} = 65 K) that undergoes a rearrangement in the magnetic structure at 65 K, while $SrCaFeOsO_6$ and Ca_2FeOsO_6 are monoclinic ferrimagnets (T_C = 210 and 350 K, respectively). All three compounds are Mott insulators that show variable range hopping conductivity, although the ferrimagnetic Ca_2FeOsO_6 is approximately 4 orders of magnitude more conducting than antiferromagnetic Sr_2FeOsO_6. The magnetic ground state is determined by competing superexchange pathways that can be controlled using chemical pressure to alter the Fe−O−Os bond angles. This work further adds to our developing understanding of superexchange coupling in transition metal oxides containing both 3d and 5d ions.

ASSOCIATED CONTENT

Supporting Information

Refined NPD patterns, refinement parameters, and temperature dependence of bond angles and unit cell volume in Sr_2FeOsO_6. This material is available free of charge via the Internet at http://pubs.acs.org.

AUTHOR INFORMATION

Corresponding Author

*E-mail: woodward@chemistry.ohio-state.edu.

Notes

The authors declare no competing financial interest.

ACKNOWLEDGMENTS

Support for this research was provided by a Materials World Network Grant funded by the National Science Foundation (award no. DMR-1107637). Partial support was supplied by the Center for Emergent Materials an NSF Materials Research Science and Engineering Center (DMR-0820414). A portion of this research was carried out at Oak Ridge National Laboratory's Spallation Neutron Source, which is sponsored by the U.S. Department of Energy, Office of Basic Energy Sciences. The authors thank Ashfia Huq for assistance with the neutron diffraction experiments. Use of the Advanced Photon Source was supported by the U.S. Department of Energy, Office of Science, Office of Basic Energy Sciences, under contract no. DE-AC02-06CH11357.

REFERENCES

(1) King, G.; Woodward, P. M. *J. Mater. Chem.* **2010**, *20*, 5785−5796.
(2) Kobayashi, K.-I.; Kimura, T.; Sawada, H.; Terakura, K.; Tokura, Y. *Nature* **1998**, *395*, 677−680.
(3) Alamelu, T.; Varadaraju, U. V.; Venkatesan, M.; Douvalis, A. P.; Coey, J. M. D. *J. Appl. Phys.* **2002**, *91*, 8909−8911.
(4) Kato, H.; Okuda, T.; Okimoto, Y.; Tomioka, Y.; Takenoya, Y.; Ohkubo, A.; Kawasaki, M.; Tokura, Y. *Appl. Phys. Lett.* **2002**, *81*, 328−330.
(5) Krockenberger, Y.; Mogare, K.; Reehuis, M.; Tovar, M.; Jansen, M.; Vaitheeswaran, G.; Kanchana, V.; Bultmark, F.; Delin, A.; Wilhelm, F.; Rogalev, A.; Winkler, A.; Alff, L. *Phys. Rev. B* **2007**, *75*, 020404(R).
(6) Kanamori, J.; Terakura, K. *J. Phys. Soc. Jpn.* **2001**, *70*, 1433−1434.
(7) Sleight, A. W.; Weiher, J. F. *J. Phys. Chem. Solids* **1979**, *33*, 679−687.
(8) Patterson, F.; Moeller, C.; Ward, R. *Inorg. Chem.* **1963**, *2*, 196−198.
(9) Ramesha, K.; Thangadurai, V.; Sutar, D.; Subramanyam, S. V.; Subbanna, G. N.; Gopalakrishnan, J. *Mater. Res. Bull.* **2000**, *33*, 559−565.
(10) Goodenough, J. B. *Phys. Rev.* **1955**, *100*, 564−573.
(11) Kanamori, J. *J. Phys. Chem. Solids* **1959**, *10*, 87−98.
(12) Sleight, A. W.; Longo, J.; Ward, R. *Inorg. Chem.* **1962**, *1*, 245−250.
(13) Paul, A. K.; Jansen, M.; Yan, B.; Felser, C.; Reehuis, M.; Abdala, P. M. *Inorg. Chem.* **2013**, *52*, 6713−6719.
(14) Morrow, R.; Mishra, R.; Restrepo, O. R.; Ball, M. R.; Windl, W.; Wurmehl, S.; Stockert, U.; Büchner, B.; Woodward, P. M. *J. Am. Chem. Soc.* **2013**, *135*, 18824−18830.
(15) Paul, A. K.; Reehuis, M.; Ksenofontov, V.; Yan, B.; Hoser, A.; Tobbens, D. M.; Adler, P.; Jansena, M.; Felser, C. *Phys. Rev. Lett.* **2013**, *111*, 167205.
(16) Feng, J. L.; Arai, M.; Matsushita, Y.; Tsujimoto, Y.; Guo, Y.; Sathish, C. I.; Wang, X.; Yuan, Y.; Tanaka, M.; Yamaura, K. *J. Am. Chem. Soc.* **2014**, *136*, 3326−3329.
(17) Huq, A.; Hodges, J. P.; Gourdon, O.; Heroux, L. *Z. Kristallogr. Proc.* **2011**, *1*, 127−135.
(18) Larson, A. C.; Von Dreele, R. B. *Los Alamos National Laboratory Report LAUR* **2000**, 86−748.
(19) Toby, B. H. *J. Appl. Crystallogr.* **1991**, *34*, 210−213.
(20) Kobayashi, K.; Nagao, T.; Ito, M. *Acta Cryst., Sect. A* **1991**, *67*, 473−480.
(21) Woodward, P. M.; Hoffmann, R.-D.; Sleight, A. W. *J. Mater. Res.* **1994**, *9*, 2118−2127.
(22) Sears, V. W. Scattering Lengths for Neutrons. In *International Tables for Crystallography*, 3rd ed.; Prince, E., Ed.; International Union of Crystallography: Chester, England, 2004; Vol. *C*, pp 444−45.
(23) Feng, H. L.; Tsujimoto, Y.; Guo, Y.; Sun, Y.; Sathish, C. I.; Yamaura, K. *High Pressure Res.* **2013**, *33*, 221−228.
(24) Macquart, R.; Kim, S. J.; Gemmill, W. R.; Stalick, J. K.; Lee, Y.; Vogt, T.; Zur Loye, H. C. *Inorg. Chem.* **2005**, *44*, 9676−9683.
(25) Retuerto, M.; Martínez-Lope, M. J.; García-Hernández, M.; Fernández-Díaz, M. T.; Alonso, J. A. *Eur. J. Inorg. Chem.* **2008**, *4*, 588−595.
(26) Lufaso, M. W.; Barnes, P. W.; Woodward, P. M. *Acta Cryst., Sect. B* **2006**, *62*, 397−410.
(27) Shannon, R. D. *Acta Cryst., Sect. A* **1976**, *32*, 751−767.
(28) Brese, N. E.; O'Keefe, M. *Acta Cryst., Sect. B* **1991**, *47*, 192−197.
(29) Mott, N. F. *Philos. Mag.* **1969**, *19*, 835.

(30) Fisher, M. E. *Philos. Mag.* **1962**, *7*, 1731.
(31) Viola, M. C.; Martinez-Lope, M. J.; Alonso, J. A.; De Paoli, J. M.; Pagola, S.; Pedregosa, J. C.; Fernandez-Diaz, M. T.; Carbonio, R. E. *Chem. Mater.* **2003**, *15*, 1655−1663.
(32) Ivanov, S. A.; Eriksson, S. G.; Tellgren, R.; Rundlöf, H.; Tseggai, M. *Mater. Res. Bull.* **2005**, *40*, 840−849.
(33) Sakaia, N.; Fjellvâga, H.; Haubackb, B. C. *J. Solid State Chem.* **1996**, *121*, 202−213.
(34) Tsushima, K.; Aoyagi, K.; Sugano, S. *J. Appl. Phys.* **1970**, *41*, 1238−40.